Time Domain Performance Evaluation of UWB Antennas

Gopikrishna Madanan and Deepti Das Krishna

Abstract

The performance of printed wideband antennas has to be optimized both in frequency and time domains, to qualify for UWB applications. This is especially true in multi-resonant antenna topologies where the excitation of different modes can change phase centers and radiation patterns with frequency. The study presented in this chapter intends to demonstrate the simulation and experimental design for the time domain characterization of UWB antennas. Modeling the antenna as a linear time-invariant system with transfer function and impulse response, distortion caused to a nanosecond pulse is analyzed. Two planar monopole antenna designs are considered for the comparative study: the SQMA and RMA. SQMA is a traditional CPW-fed monopole design with ground modifications for ultra wide-bandwidth. RMA is a rectangular CPW-fed monopole with an impedance transformer arrangement at the antenna feed. RMA maintains constant impedance over the entire UWB and contributes towards maintaining uniformity in the radiation patterns over the entire frequency band by its design. Transfer function measurements are performed for both the azimuthal and elevation planes and the impulse responses are deduced by performing IFFT. Parameters such as FWHM and ringing are computed from the impulse response for the performance comparison. To evaluate the influence of the antenna geometry on a transmitted/received pulse, the impulse responses are convoluted with a standard UWB pulse. The time-domain distortion for the designs is then compared by computing the Fidelity parameter.

Keywords: ultra wide band, planar monopole antenna, antenna transfer function, antenna impulse response, time domain analysis

1. Introduction

Ultra-wide band systems transmit and receive ultra-short electromagnetic pulses having limited effective radiated power. The system performance is determined primarily by the characteristics of the radiators that have to conform with stringent frequency and time domain requirements in the entire operating band [1]. These requirements are namely, a non-dispersive phase centre; constant radiation and impedance over the frequency range with no excitation of higher order modes [2]. Planar monopole antennas with wide operating bands are most often well matched multi-resonant structures. In [3], Ma et al. have described the time domain performance of a printed dipole antenna employing a tapered slot feed. It is reported that the received pulses are distorted and broadened to more than 1 ns in spite of the antenna being well matched over the entire band. The higher order modes generated tends to shift the antenna phase centers with frequency and can lead to

broadening of the radiated pulse. The same authors in [4] reports a much lesser pulse distortion for a tapered slot antenna operating in the 3.1–10.6 GHz UWB band. The present chapter intends to outline the design, simulation and measurement steps followed to characterize UWB antennas in the time domain.

Two monopole antennas with similar design topology is considered for the present analysis: the SQMA with a square radiator and RMA with a rectangular radiator. In both the antennas, the ground plane is optimally designed for a wide impedance bandwidth. The general practice to realize ultra wide-bandwidth in square/rectangular radiating elements is to modify the ground–radiator interface [5–10]. In SQMA, the inherent resonances of a square patch is matched over the wide band by incorporating cuts in the ground plane at specific locations [11]. The designs proposed in [11, 12] have been contemplated to design the RMA. In RMA, the PCB footprint is greatly reduced and radiation patterns in the 3.1–10.6 UWB is stable without much radiation squinting which is otherise observed in wideband antennas at higher frequencies primarily due to the current distribution on the antenna ground plane [13]. Incase of RMA, this aspect is taken into consideration in the design ensuring broadside radiation all through the band of operation. This is further confirmed from the spatio-temporal transfer characteristics and the transient response analysis, making it suitable for UWB applications.

2. Time domain analysis

Antennas intended for UWB systems need to possess superior pulse handling capabilities. Analysis of the transient response of the antenna is performed by direct time domain measurements [14, 15] or by a frequency domain measurement followed by Fourier Transformation [16, 17]. Frequency domain measurements take advantage of the high dynamic range and the standardized calibration of the vector network analyzer and is equally accurate to the direct time domain measurements.

In the latter method, the antenna is considered as a linear time invariant system described by its transfer function (gain and phase) and the associated impulse response [18, 19]. Transfer function and impulse response of UWB antennas are modeled as spatial vectors as the antenna characteristics depend on the signal propagation direction [16, 17]. **Figure 1** shows the model for the analysis which consists of a radio link made up of two antennas in free space under the approximation of far–field and line-of-sight propagation. In this model, the transmitting and receiving antennas are characterized by eliminating channel effects [20].

2.1 Transient reception

The time domain relation between the received voltage pulse $\vec{U}_{Rx}(\omega, r, \theta, \varphi)$ and the incident electric field pulse $\vec{E}_{rad}(\omega, r, \theta, \varphi)$ is [17],
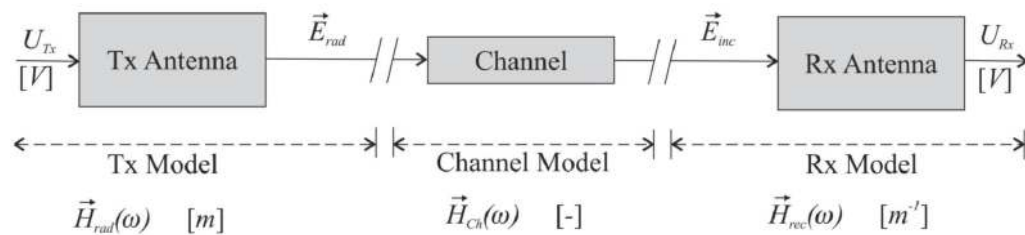

Figure 1.
The UWB channel model.

$$\frac{\vec{U}_{Rx}(\omega, r, \theta, \varphi)}{\sqrt{z_c}} = \vec{h}_{Rx}(\omega, \theta, \varphi) \frac{\vec{E}_{rad}(\omega, r, \theta, \varphi)}{\sqrt{z_0}} \tag{1}$$

In the time domain, the corresponding relation is,

$$\frac{\vec{u}_{Rx}(t, r, \theta, \varphi)}{\sqrt{z_c}} = \vec{h}_{Rx}(t, \theta, \varphi) \otimes \frac{\vec{e}_{rad}(t, r, \theta, \varphi)}{\sqrt{z_0}} \tag{2}$$

z_c and z_0 are the antenna port and free–space characteristic impedance respectively, while $\otimes$ indicates convolution operation. If (θ, φ) represents the elevation and azimuth angles, the receive antenna transfer function $\vec{h}_{Rx}(\omega, \theta, \varphi)$ and its impulse response $\vec{h}_{Rx}(t, \theta, \varphi)$ are considered as a function of the angle of arrival of the received pulse.

An ideal receiving antenna should receive a voltage pulse of the same shape as the one incident on it from any direction. This means that it should have a Dirac–delta impulse response which is also be independent of the angle of arrival. In other words, the antenna transfer function should have a uniform amplitude and a linear phase response (or constant group delay). However, in practice, the receiving antenna transfer function is always band limited.

2.2 Transient radiation

The frequency domain relation between the transmitted electric field pulse and the applied voltage pulse is,

$$\frac{\vec{E}_{rad}(\omega, r, \theta, \varphi)}{\sqrt{z_0}} = \vec{h}_{Tx}(\omega, \theta, \varphi) \frac{e^{-j\omega r/c}}{r} \frac{U_{Tx}(\omega, r, \theta, \varphi)}{\sqrt{z_c}} \tag{3}$$

and,

$$\vec{h}_{Tx}(\omega, \theta, \varphi) = \frac{j\omega}{2\pi c} \vec{h}_{Rx}(\omega, \theta, \varphi) \tag{4}$$

The time domain relation between the transmitted electric field pulse $\vec{e}_{rad}(t, r, \theta, \varphi)$ and the applied voltage pulse $\vec{u}_{Tx}(t, r, \theta, \varphi)$ at the transmitting antenna is,

$$\frac{\vec{e}_{rad}(t, r, \theta, \varphi)}{\sqrt{z_0}} = \frac{1}{r} \partial\left(t - \frac{r}{c}\right) \otimes \left[\frac{1}{2\pi c} \frac{\partial}{\partial t} \vec{h}_{Rx}(t, \theta, \varphi)\right] \otimes \frac{u_{Tx}(t, r, \theta, \varphi)}{\sqrt{z_c}} \tag{5}$$

where,

$$\vec{h}_{Tx}(t, \theta, \varphi) = \frac{1}{2\pi c} \frac{\partial}{\partial t} \vec{h}_{Rx}(t, \theta, \varphi) \tag{6}$$

The convolution with the delta function in Eq. (5) represents the time delay attributed to the finite speed of light, denoted by c. Eq. (6) indicates that the transmit impulse response $\vec{h}_{Tx}(t, \varphi)$ is a time derivative of the receive impulse response $\vec{h}_{Rx}(t, \theta, \varphi)$. As a result, an ideal antenna (with $\vec{h}_{Rx}(t, \theta, \sigma) = \delta(t)$) will radiate an electric field pulse which would be a first–order time derivative of the input voltage pulse.

2.3 Model of transient transmission

The full input-to-output characteristics, in both frequency and time domains is deduced from 1 and 3 as below,

$$\frac{\vec{U}_{Rx}(\omega,r,\theta,\varphi)}{U_{Tx}(\omega,r,\theta,\varphi)} = \vec{A}_{Tx,Rx} \, \frac{e^{-j\omega r/c}}{r} \, \vec{h}_{Rx}(\omega,\theta,\varphi)$$

$$= \sqrt{\frac{2\omega}{c}} \, \vec{A}_{Tx,Rx} \, \frac{c \, e^{-j\omega r/c}}{2r\omega} \, \sqrt{\frac{2\omega}{c}} \, \vec{h}_{Rx}(\omega,\theta,\varphi)$$

(7)

where,

$$\vec{A}_{Tx,Rx} = \frac{j\omega}{2\pi c} \, \vec{h}_{Rx}(\omega,\theta,\varphi)$$

$$S_{21}(\omega) = \frac{\vec{U}_{Rx}(\omega,r,\theta,\varphi)}{U_{Tx}(\omega,r,\theta,\varphi)} = \vec{H}_{Tx}(\omega,\theta,\varphi) \, H_{Ch}(\omega) \, \vec{H}_{Rx}(\omega,\theta,\varphi) \qquad (8)$$

where,

$$\vec{H}_{Tx}(\omega,\theta,\varphi) = \sqrt{\frac{2\omega}{c}} \, \vec{A}_{Tx,Rx} \tag{9}$$

$$H_{Ch}(\omega) = \frac{c \, e^{-j\omega r/c}}{2r\omega} \tag{10}$$

$$\vec{H}_{Rx}(\omega,\theta,\varphi) = \sqrt{\frac{2\omega}{c}} \, \vec{h}_{Rx}(\omega,\theta,\varphi) \tag{11}$$

In the time domain, 7 reads,

$$\frac{\vec{u}_{Rx}(t,r,\theta,\varphi)}{u_{Tx}(t,r,\theta,\varphi)} = \vec{h}_{Tx}(t,\theta,\varphi) \otimes h_{Ch}(t) \otimes \vec{h}_{Rx}(t,\theta,\varphi) \tag{12}$$

2.4 Simulation

For the time domain characterization of the antennas, the fourth derivative of the Gaussian pulse given in Eq. (13) and shown in **Figure 2(a)** is chosen as the input pulse, as this pulse conforms to the FCC spectral mask as shown in **Figure 2(b)** when A = 0.333 and T = 0.175 nS.

$$s_i(t) = A \cdot \left[3 - 6\left(\frac{4\pi}{T^2}\right)(t-\tau)^2 + \left(\frac{4\pi}{T^2}\right)^2 (t-\tau)^4\right] e^{-2\pi\left(\frac{t-\tau}{T}\right)^2} \quad \left(\frac{V}{m}\right) \tag{13}$$

For the antennas discussed in the later sections of this chapter, the input voltage $u_{Tx}(t)$ (= $s_i(t)$) is specified in CST Microwave Studio and the radiated pulse $\vec{e}_{rad}(t,r,\theta,\varphi)$ is calculated on a sphere of radius 25 cm. Fourier transforms of these two quantities are then calculated and the transfer function $\vec{H}_{Rx}(\omega,\theta,\varphi)$ is
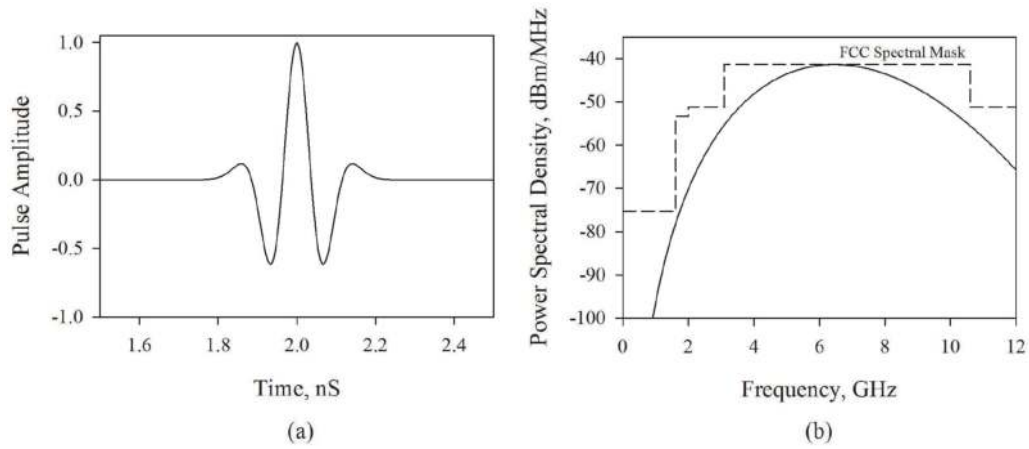
Figure 2.
(a) Input pulse (b) power spectral density.

deduced from Eq. (4). An IFFT operation on this would generate the pulse response $\vec{h}_{Rx}(t, \theta, \varphi)$.

2.5 Measurement

A scattering parameter S_{21} measurement in the frequency domain can be used to deduce the transfer functions of both the transmitting and receiving antennas. Two identical standared horn antennas oriented in the bore sight direction is used, and considering Eq. (7), the corresponding transfer functions are found out from

$$H_{Tx}(\omega, \theta, \varphi) = \sqrt{\frac{j}{2\pi} \left(\frac{\omega}{c}\right)^2 \frac{S_{21}(\omega, \theta, \varphi)}{H_{Ch}(\omega, \theta, \varphi)}} \qquad (m^{-1}) \qquad (14)$$

$$H_{Rx}(\omega, \theta, \varphi) = \sqrt{\frac{2\pi}{j} \left(\frac{c}{\omega}\right)^2 \frac{S_{21}(\omega, \theta, \varphi)}{H_{Ch}(\omega, \theta, \varphi)}} \qquad (m) \qquad (15)$$

where the free space transfer function is,

$$H_{Ch}(\omega) = \frac{c}{2d\omega} \, exp\left(\frac{-j\omega d}{c}\right) \qquad (16)$$

Once the reference antenna (Tx Antenna) is characterized, transfer function of the AUT is found for multiple orientations using,

$$H_{AUT}(\omega, \theta, \varphi) = \frac{S_{21}(\omega, \theta, \varphi)}{H_{Tx}(\omega)H_{Ch}(\omega)} \qquad (17)$$

2.6 Data processing, windowing

S_{21} is measured with frequency resolution 15.25 MHz and Eqs. (14)–(17) are used to compute the corresponding transfer functions. The data is further appended with zero padding for 0–2 GHz and 12–62.47 GHz range with 4096 points in the pass band. The conjugate of this signal is is then reflected to the negative frequencies to get a double sided spectrum of a real signal which is then transformed to the time domain using IFFT.

Measurements using two identical wide band horns are shown in **Figure 3**. While **Figure 3(a)** represents the measured antenna transfer functions, **Figure 3(b)** shows the real and imaginary parts of the transfer functions. Transmitting and receiving antenna impulse responses are shown in **Figure 3(c)** which clearly indicates that $\vec{h}_{Tx}(t)$ is a derivative of $\vec{h}_{Rx}(t)$.

2.7 Time domain parameters

The time domain evaluation of the antenna effects on the transmitted/received signals is carried out by analyzing the envelope of the analytic response for co–polarization. The real valued antenna's transient response is,

$$h_n(t) = \Re \vec{h}_n(t) \tag{18}$$

The peak output voltage from an incident wave form depends on the peak value $p(\theta, \varphi)$ of the antenna's transient response:

$$p(\theta, \varphi) = \max_t \left| \vec{h}_n(t, \theta, \varphi) \right| \tag{19}$$

A measure for the linear distortion of the antenna is the envelope width, which is defined as the full width at half maximum (FWHM) of the magnitude of the transient response envelope.
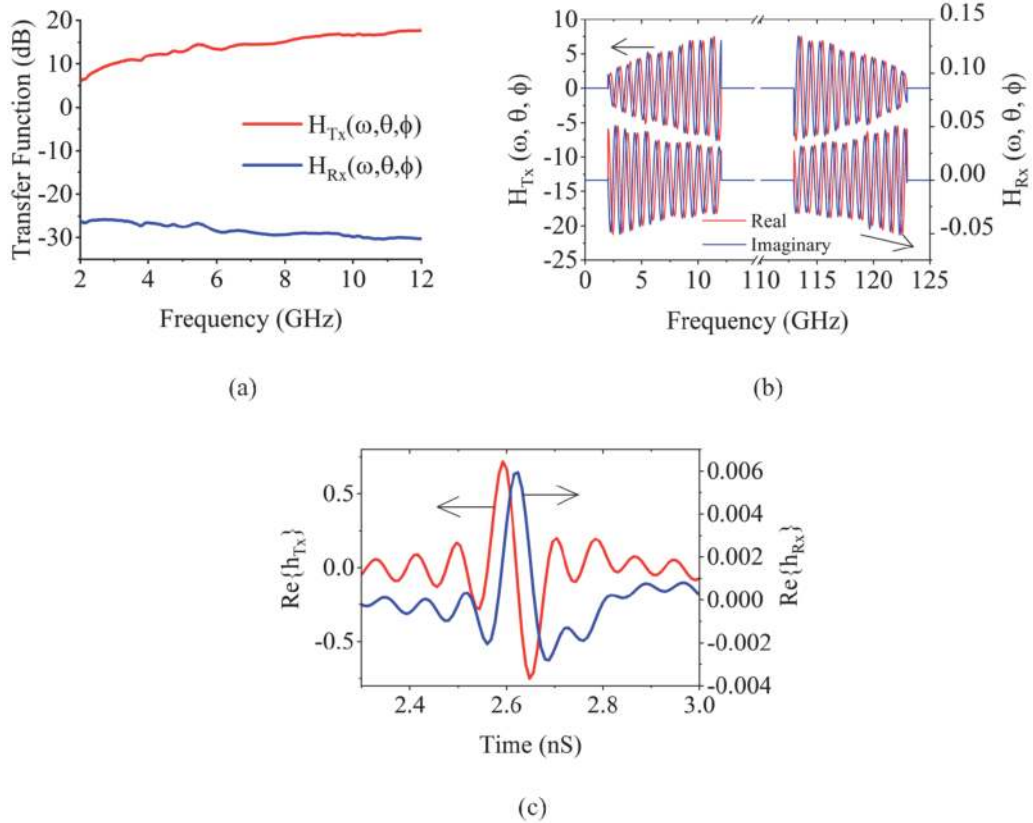

(a)

(b)

(c)

Figure 3.
(a) Transmitting and receiving transfer functions of identical wide band horn antennas (b) transmitting and receiving transfer functions after conjugate reflection (c) impulse response of the transmitting antenna and receiving antenna.

$$FWHM_{0.5}(\theta, \varphi) = t_2\big|_{p/2} - t_1\big|_{p/2, t_1 < t_2} \qquad (20)$$

The duration of the ringing is defined as the time until the envelope has fallen from the peak value below a fraction α of the main peak.

$$RINGING_\alpha = t_2\big|_{\alpha \cdot p} - t_1\big|_{p, t_1 < t_2} \qquad (21)$$

The lower bound for α is chosen according to the noise floor of the measurement. In order to compare the ringing of antennas with different gains under the condition of a constant noise floor, the fraction α is chosen to be 0.22 (-13 dB).

2.8 Pulse distortion analysis

The antenna effects on the received signal is evaluated by convoluting the analytic response $\vec{h}_n(t, \theta, \varphi)$ with the input pulse $s_i(t)$.

$$s_o(t) = \vec{h}_n(t, \theta, \varphi) \otimes s_i(t) \qquad (22)$$

For UWB systems, receivers are in general based on the pulse energy detection or correlation with the template waveform. Therefore, the pulse distortions can be examined by calculating fidelity factor which is defined as [21],

$$F = max \quad \frac{\int_{-\infty}^{+\infty} s_i(t) \cdot s_o(t - \tau)\, dt}{\sqrt{\int_{-\infty}^{+\infty} |s_i(t)^2|\, dt \cdot \int_{-\infty}^{+\infty} |s_o(t)^2|\, dt}} \qquad (23)$$

where τ is the delay parameter varied in a sense to maximize the numerator. The fidelity parameter measurement is performed for different spatial orientations of the test antenna and is evaluated as the maximum of the cross–correlation function. It compares only shapes of the waveforms, not amplitudes.

3. Performance comparison of UWB antennas

To demonstrate the necessity of the time domain analysis of UWB antennas, two topologies shown in **Figure 4** is considered.

3.1 Antenna designs

Figure 4(a) depicts the design of the SQMA. The overall length of the element determines the lower end of the operational band and the upper end by the feed gap 'd'. It is the ground plane which determines the impedance bandwidth of a monopole antenna. In the present design, the cuts engraved in the ground plane match the multiple resonances, making the antenna operate over the specified ultra wide band. The SQMA has the following dimensions with units of lengths in mm: $s = 2.3, g = 0.48, l\_patch = 16, l = 14.57, b = 13, d = 0.5, w = 1.4, L = 32, W = 30, \varepsilon_r = 4.4, tan(\delta) = 0.02, h = 1.6$.

The topology of the RMA comprises of a rectangular monopole of area $l_1 \times b_1$ as shown in **Figure 4(b)**. This antenna is evolved from a basic printed monopole design shown in the same Figure. To facilitate ultra wide band performance, an impedance transformer is embedded in the CPW transmission line with increasing slot widths g_1, g_2, g_3 and g_4. The special design of the transformer provide gradual transformation of the 50 Ω line impedance and at the same time, result in a new current path for
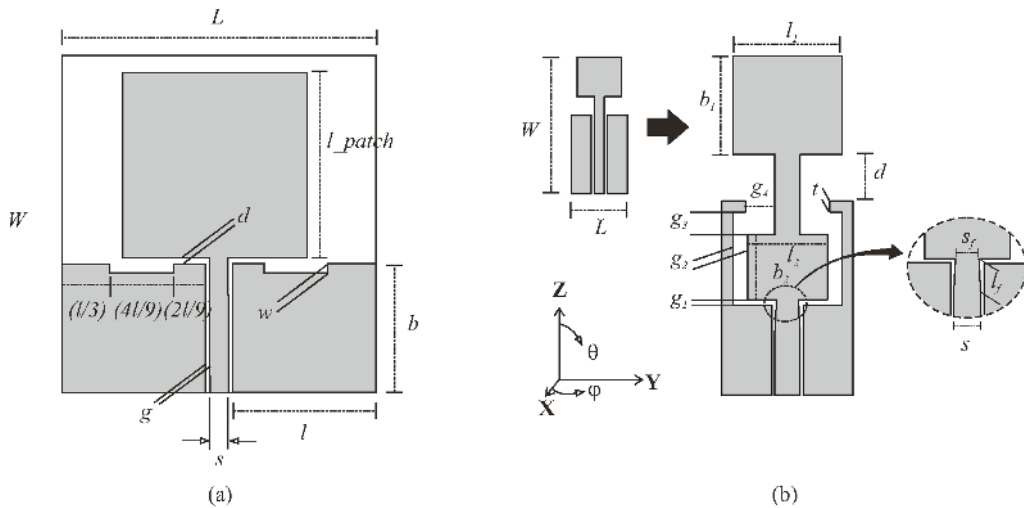
Figure 4.
Design and parameters of (a) SQMA (b) RMA.

radiation. The coupling of the guided waves to the radiator is strongly dependent on parameter d and the resonances in the structure can be matched by suitably choosing d. For the RMA, the geometric parameters are: $s = 2.3, g = 0.28, d = 4.25, l_1 = 9, b_1 = 10, l_g = 17.75, l_2 = 6, b_2 = 7.3, g_1 = 0.45, g_2 = 1.35, g_3 = 2, g_4 = 2.7, t = 1, s_f = 2, l_f = 3, L = 30, W = 12, \varepsilon_r = 4.4, tan(\delta) = 0.02, h = 1.6$. Unit of all lengths are in *mm*.

3.2 Performance evaluation in the frequency domain

Measured and simulated return losses of the two antennas are shown in **Figure 5**. The prominent resonances in the SQMA are at 3.8 GHz, 8 GHz and
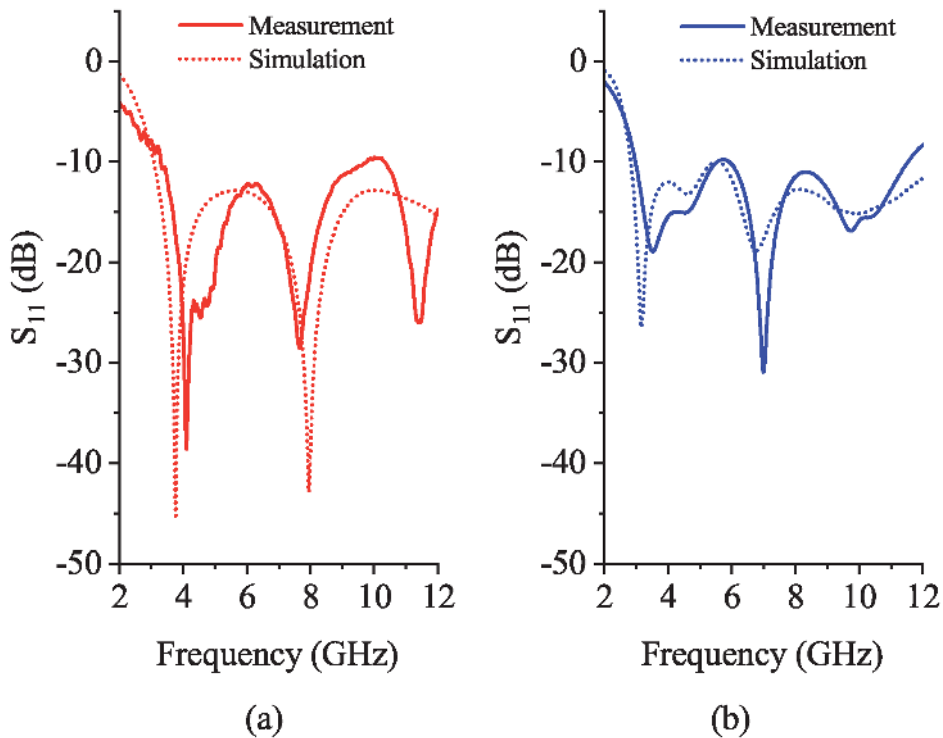
Figure 5.
Measured and simulated S_{11}(dB) of the (a) SQMA and (b) RMA.

13 GHz while that for the RMA are at 3.5 GHz, 5 GHz, 7 GHz and 11 GHz. Both antennas cover the 3.1-10.6 GHz UWB.

3-D radiation patterns of the two antennas obtained from CST are shown in **Figure 6**. In SQMA, the pattern degradation at the higher frequencies were found to be effective from 8 GHz onwards. SQMA also shows pattern squinting as in **Figure 6(a)**. For the RMA, the pattern degradation at the higher frequencies are minimum; radiation is stable and directed towards the bore-sight at all frequencies. The cross–polar level exhibited by both the antennas remain better than −20 dB in the 3.1–10.6 GHz band. Both antennas have linear polarization, oriented in the Z direction. Peak gains of the antennas were measured by gain transfer method. Average value of the peak gain in the 3.1–10.6 GHz UWB is found to be 3.75 dBi for SQMA and 2.6 dBi for the RMA.

3.3 Performance evaluation in the time domain

As an UWB signal is transmitted or received, the pulse shape is altered. This distortion is reflected in the transfer function (in the frequency domain) or impulse response (in the time domain) of the antenna. The antenna transfer function, a complex quantity, would have a constant amplitude and linear phase response while the impulse response would be a delta function, in cases when the antenna has no effect on the pulse transmitted.

3.3.1 Results of simulation in CST

Magnitude of the transfer function $\vec{h}_{Rx}(\omega, \theta, \varphi)$ simulated in CST for the x-y plane of the antennas are shown in **Figure 7(a)** (Using Eq. (3)). It is seen that the intensity plots for $\vec{h}_{Rx}(\omega, \theta, \varphi)$ and $\vec{h}_{Tx}(\omega, \theta, \varphi)$ differ only in their relative
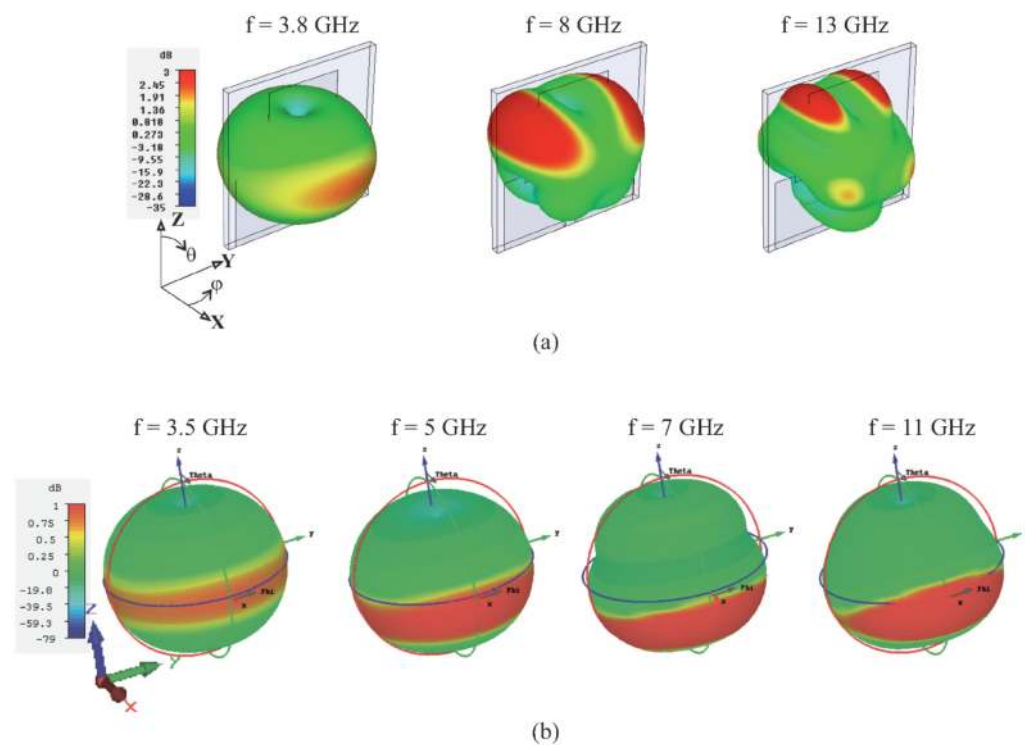

Figure 6.
Simulated radiation patterns at different frequencies for the the antennas (a) SQMA (b) RMA.

amplitudes. Magnitude of the transfer function decay gradually as a function of frequency over most of the azimuth angles (x-y plane). The loss of omni-directionality of the pattern of SQMA at frequencies above 8 GHz is reflected in its transfer function as relatively low intensities at at certain angles. Sharp nulls are seen between 30^0–50^0, 130^0–150^0, 210^0–230^0 and 320^0–330^0. Transfer function in the x-z plane of the SQMA is shown in **Figure 7(b)**. The nulls in the radiation
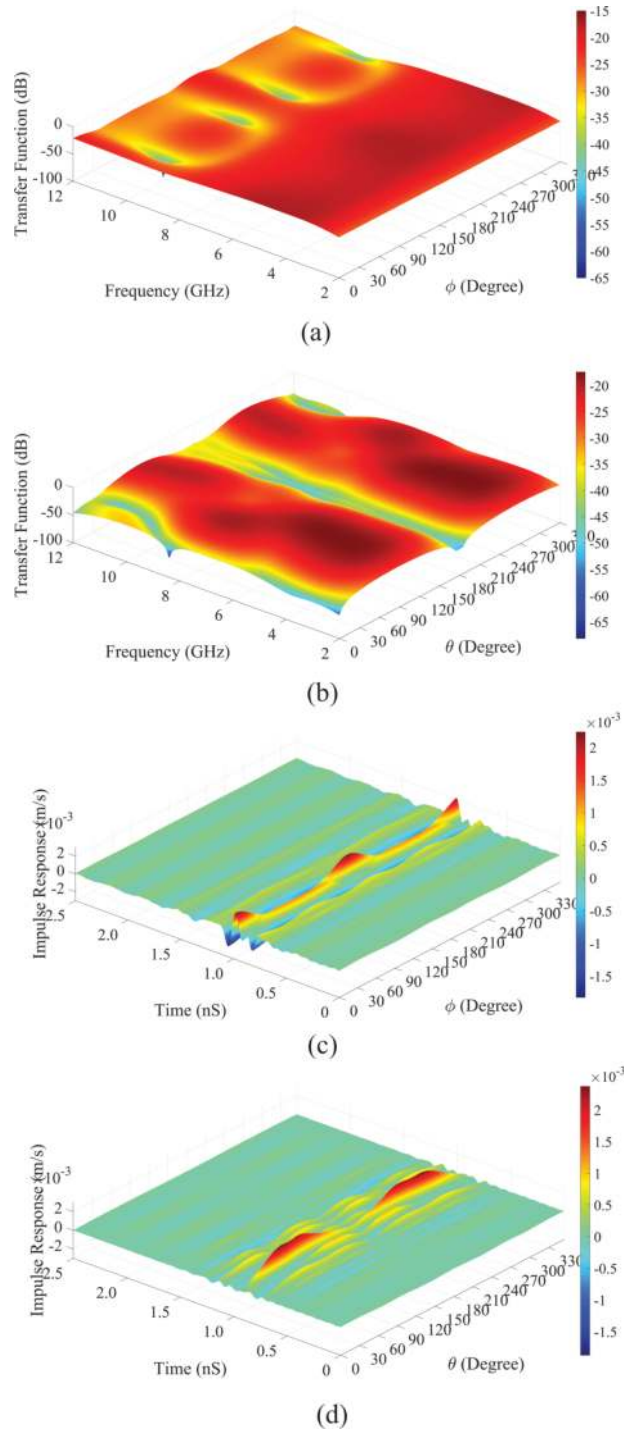
Figure 7.
Computed transfer functions of the SQMA in the (a) x-y (b) x-z planes; computed impulse responses the SQMA in the (c) x-y (d) x-z planes.

pattern at 180^0 can be seen in the transfer functions which show intensity variations.

Impulse response in the x-y plane is well formed with good peak value over almost all the angular regions as shown in **Figure 7(c)**. Amplitude degradation beyond 8 GHz in the SQMA impulse response is reflected between 30^0–120^0
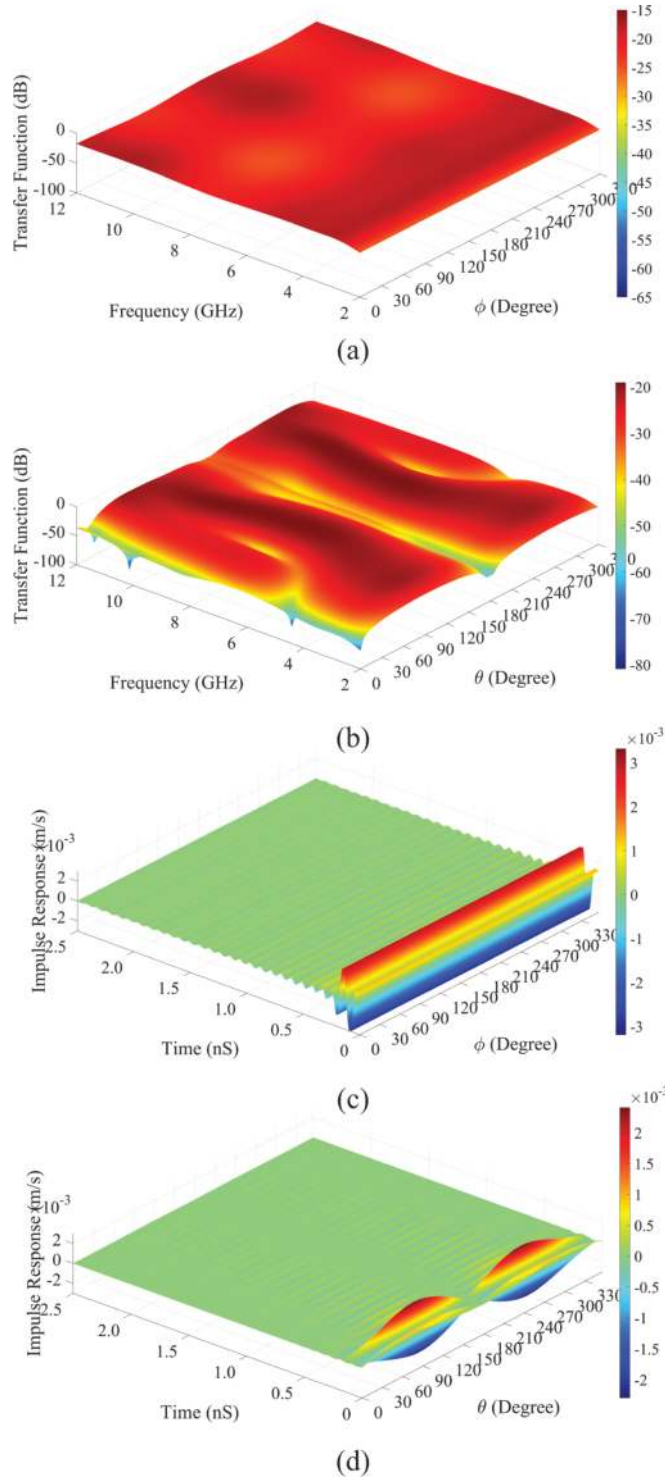

Figure 8.
Computed transfer functions of the RMA in the (a) x-y (b) x-z planes; computed impulse responses the RMA in the (c) x-y (d) x-z planes.

and 200^0–330^0. Impulse response in the x-z plane of the SQMA is shown in **Figure 7(d)**.

Figure 8(a) indicates that the antenna transfer function of the RMA in the x-y plane is fairly constant throughout the entire UWB. Even though computed transfer function in the x-z plane shown in **Figure 8(b)** has variations, it remains within the acceptable limits. The nulls observed in the transfer function in **Figure 8(b)** can be attributed to the monopole pattern of RMA. Impulse responses computed in the x-y and x-z planes for the RMA is shown in **Figure 8(c)** and **8(d)**. In the x-y plane, the impulse response preserves the expected Dirac-delta shape, unlike that in the SQMA. Even though not in the perfect shape, impulse response of the RMA in the x-z plane has more resemblance to a Dirac-delta, when compared to SQMA.
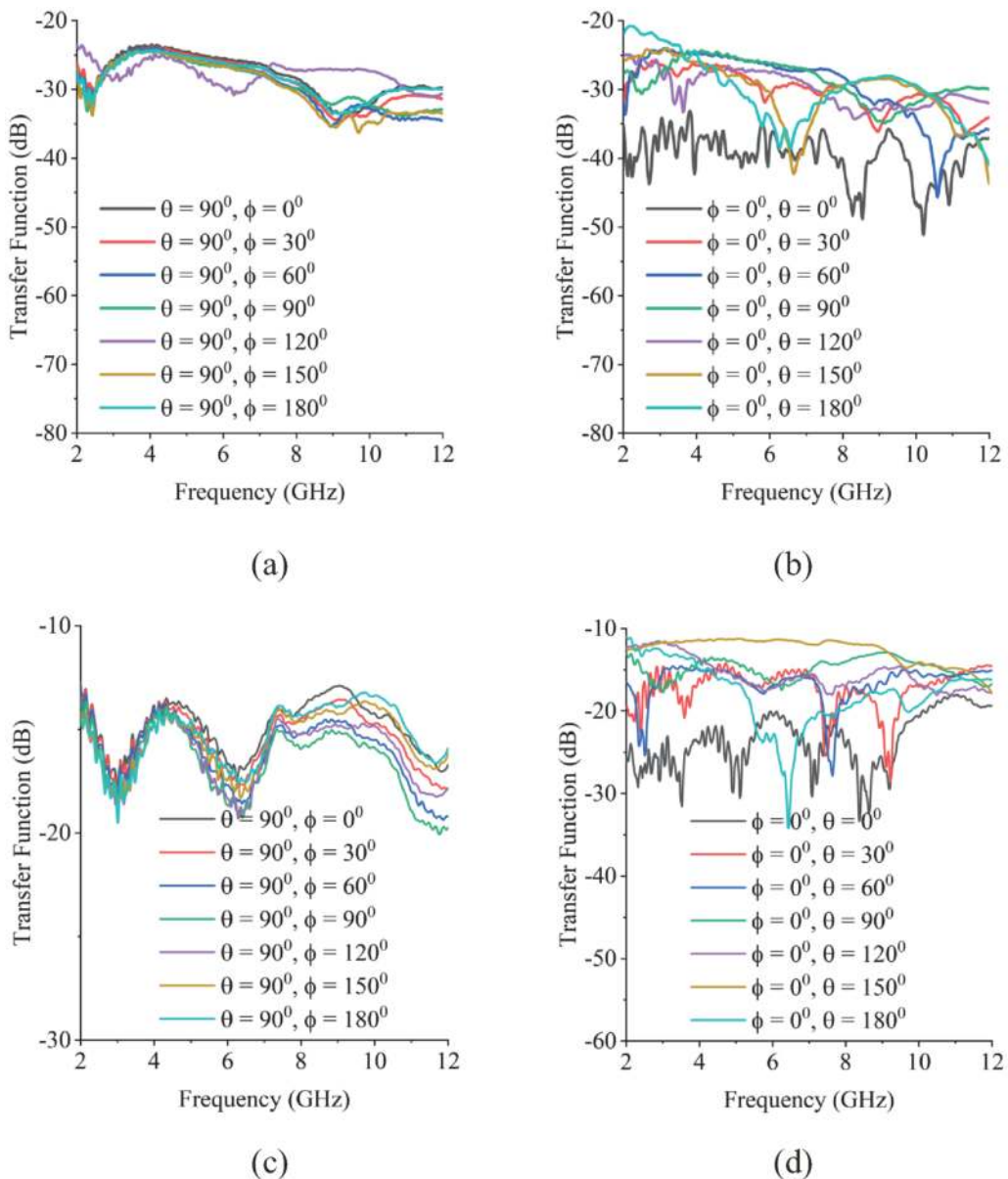

Figure 9.
Measured antenna transfer functions: (a) SQMA, x-y plane (b) SQMA, x-z plane (c) RMA, x-y plane (d) RMA, x-z plane.
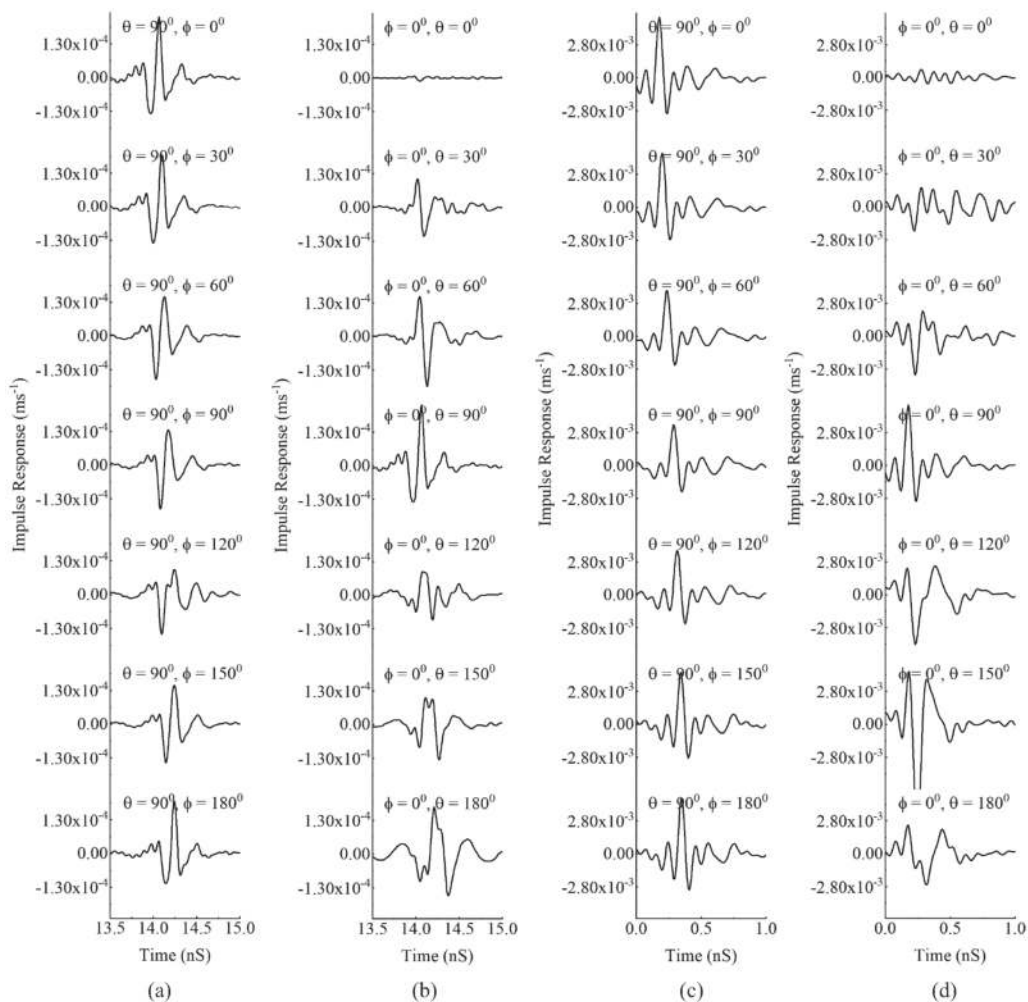
Figure 10.
Measured impulse responses: (a) SQMA, x-y plane (b) SQMA, x-z plane (c) RMA, x-y plane (d) RMA, x-z plane.

3.3.2 Experimental results

For the measurements, the transmitting and receiving antennas were positioned in their far field, at a distance of 25 cm. Source power level in the VNA was set at 10 dB to improve signal to noise ratio in the measured data.

Figure 9(a) and **(b)** indicate the measured antenna transfer functions in the x-y and x-z planes for the SQMA. The measurements seem to follow simulations indicated in Section 3.3.1. **Figure 9(c)** and **(d)** indicate the transfer functions in the x-y and x-z planes for the RMA. While the transfer functions in the x-y planes remain constant with variation within 10 dB, the measured values for the x-z plane shows large variations at particular frequencies.

The **Figure 10(a)–(d)** shows the corresponding impulse responses, obtained by performing an IFFT on the measured transfer functions and they resemble delta functions across all the angles in the x-y plane.

Figures 11 and **12** shows the time domain performance indicators of the antennas for x-y and y-z planes. For the RMA, as the **Figure 11(a)** shows, the FWHM is constant and ringing is minimum at all angles in the x-y plane. The SQMA however shows variations, though within acceptable limits, which could be attributed to its relatively larger size. Computations also futher confirms that fidelity of the received
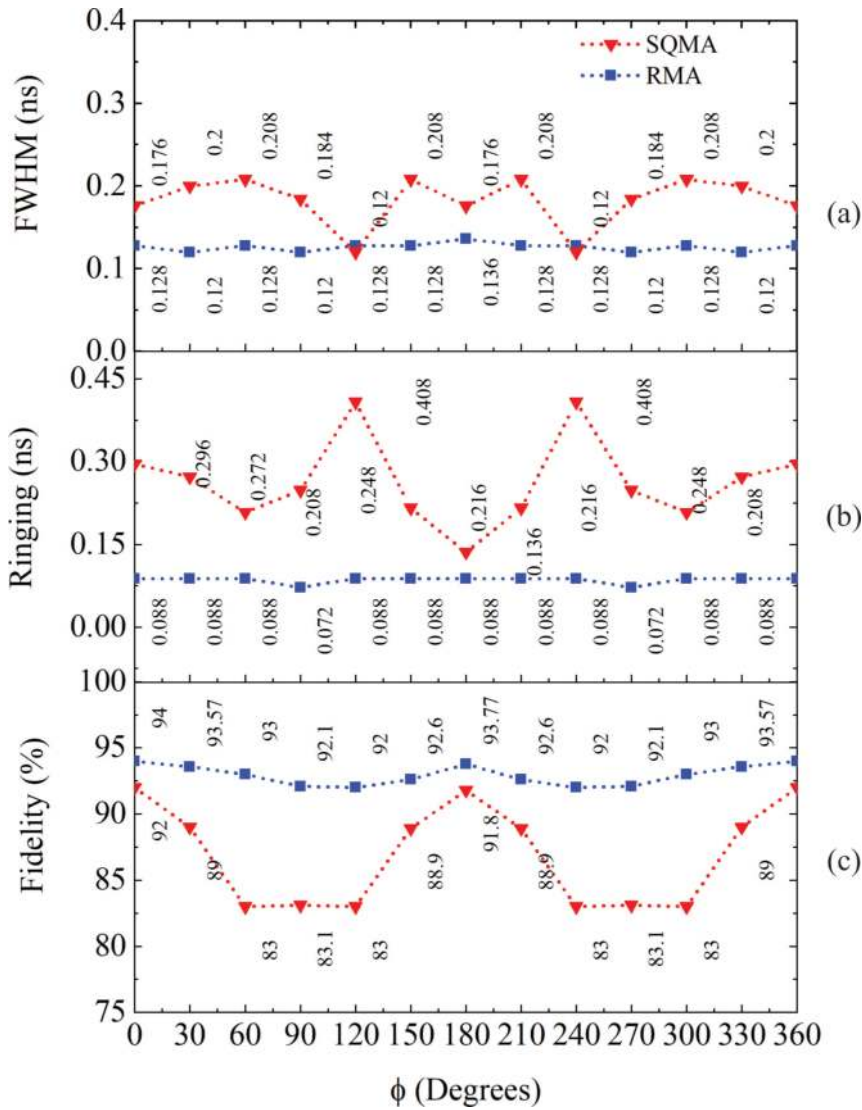
Figure 11.
Computed (a) FWHM (b) ringing and (c) Fidelity measured in the x-y plane.

pulses in the case of RMA is constant and better compared to the SQMA. The performance indicators show variations in the x-z plane in tune with the corresponding radiation patterns. Impulse responses are convoluted with the pulse form given in Eq. (13) to study the effect of the antenna geometry on a transmitted the baseband pulse. Computed fidelity of the received pulses of the RMA is constant and better compared to the SQMA. Variation in Fidelity in the $(\theta = 0^0, \phi = 0^0)$ and $(\theta = 180^0, \phi = 0^0)$ directions could be attributed to the nulls in the radiation patterns at those angles.

4. Conclusion

Printed UWB antennas are multi-resonant structures that operate over a wide frequency range. Even if the radiators designed for UWB exhibit excellent band-width, efficiency, etc., traveling phase centers present in the geometry can impair their use in time-domain applications. Changes in the antenna phase centers are reflected in the time domain as a dispersion in the transmitted/received pulses. A
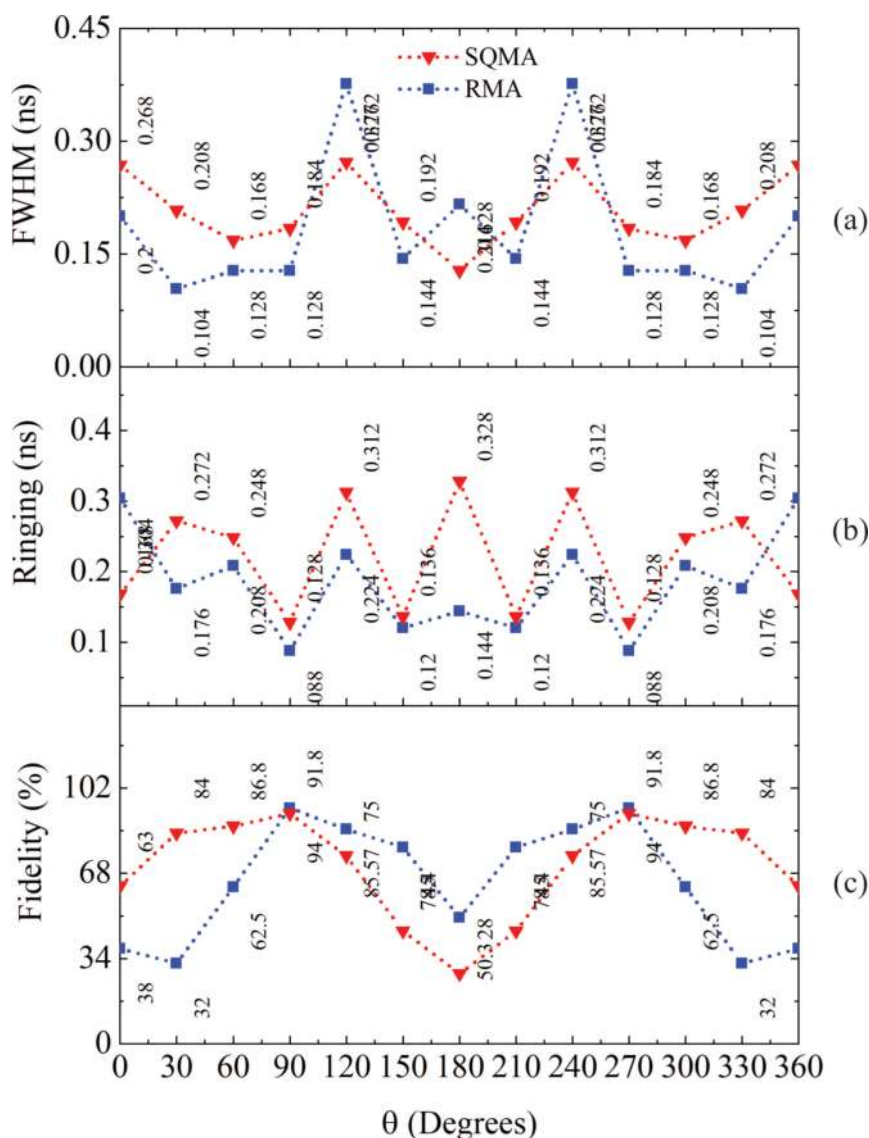
Figure 12.
Computed (a) FWHM (b) ringing and (c) Fidelity measured in the x-z plane.

variation in antenna phase center can be quantified in terms of group delay or antenna transfer function, a curb on the former being 1nS over the entire band and that on the latter is to remain within 10 dB.

In this work, we have demonstrated this point by comparing the time-domain performance of two similar antenna geometries: the SQMA and the RMA. PCB area occupied by the SQMA is approximately 2.7 times that of the RMA and resonances in the geometry are inherent due to the square patch itself. Because of the different modes that are excited in the geometry, its peak radiation points are disoriented in the higher side of the UWB. Severe pattern degradation has also been observed at these frequencies. In RMA, the radiation patterns are found to be stable with minimum degradation at the higher frequencies. The design of RMA has achieved this virtue by manipulating the surface currents in the geometry. Abrupt discontinuities that can cause reflections in the geometry are avoided by the impedance transformer designed in the ground plane.

As frequency domain characterizations hardly throw light into the pulse handling capabilities UWB antennas, a method to characterize them in the time domain

is presented in this work. Temporal characterizations of the two antennas performed by the method outlined here reveal a close correspondence between the geometry of the antenna with its performance in the time domain. From the study, it is concluded that for good time-domain performance, excitation of multiple modes within the operating band of the UWB antennas has to be taken care of during the designing of the antennas itself and its physical dimension has to remain to a minimum. The first condition minimizes internal reflections and the subsequent cancelations in the antenna geometry while the second one ensures that there are no changes in the phase center of the antenna.

Acknowledgements

The authorship criteria are listed in our Authorship Policy: https://www.intech open.com/page/authorship-policy.

Conflict of interest

The authors declare no conflict of interest.

Abbreviations

FCC   Federal Communication Commission
FWHM   Full Width Half Maxima
IFFT   Inverse Fast Fourier Transform
RMA   Rectangle Monopole Antenna
SQMA   Square Monopole Antenna
UWB   Ultra Wide-band

Author details

Gopikrishna Madanan[1*†] and Deepti Das Krishna[2†]

1 Department of Physics, Government Victoria College, Palakkad, Kerala, India

2 Department of Electronics, Cochin University of Science and Technology, Cochin, Kerala, India

*Address all correspondence to: gopikrishna@gvc.ac.in

† These authors contributed equally.

IntechOpen

References

[1] Ghosh D, De A, Taylor MC, Sarkar TK, Wicks MC, Mokole EL. Transmission and reception by ultra-wideband (UWB) antennas. IEEE Antennas and Propagation Magazine. 2006;48(5):67–99.

[2] Galvan-Tejada GM, Peyrot-Solis MA, Aguilar HJ. Ultra wideband antennas: design, methodologies, and performance. CRC Press; 2017.

[3] Ma TG, Jeng SK. A printed dipole antenna with tapered slot feed for ultrawide-band applications. IEEE Transactions on Antennas and Propagation. 2005;53(11):3833–3836.

[4] Ma TG, Jeng SK. Planar miniature tapered-slot-fed annular slot antennas for ultrawide-band radios. IEEE transactions on Antennas and Propagation. 2005;53(3):1194–1202.

[5] Chu QX, Yang YY. A compact ultrawideband antenna with 3.4/5.5 GHz dual band-notched characteristics. IEEE transactions on antennas and propagation. 2008;56(12):3637–3644.

[6] Acharjee J, Mandal K, Mandal SK, Sarkar PP. A compact printed monopole antenna with enhanced bandwidth and variable dual band notch for UWB applications. Journal of Electromagnetic Waves and applications. 2016;30(15): 1980–1992.

[7] Lee SS, Choi SS, Park JK, Cho KR. Experimental study of UWB antenna in the time domain. Microwave and Optical Technology Letters. 2005;47(6):554–558.

[8] Shameena V, Suma M, Raj Rohith K, Bybi P, Mohanan P. Compact ultra-wideband planar serrated antenna with notch band ON/OFF control. Electronics Letters. 2006;42(23):1323–1324.

[9] Wu Q, Jin R, Geng J, Lao J. Ultra-wideband rectangular disk monopole antenna with notched ground. Electronics Letters. 2007;43(11): 605–606.

[10] Li Y, Li W, Ye Q. A reconfigurable triple-notch-band antenna integrated with defected microstrip structure band-stop filter for ultra-wideband cognitive radio applications. International Journal of Antennas and Propagation. 2013;2013.

[11] Gopikrishna M, Krishna D, Chandran A, Aanandan C. Square monopole antenna for ultra wide band communication applications. Journal of Electromagnetic Waves and Applications. 2007;21(11):1525–1537.

[12] Gopikrishna M, Krishna DD, Anandan C, Mohanan P, Vasudevan K. Design of a compact semi-elliptic monopole slot antenna for UWB systems. IEEE Transactions on Antennas and Propagation. 2009;57(6):1834–1837.

[13] Fereidoony F, Chamaani S, Mirtaheri SA. UWB monopole antenna with stable radiation pattern and low transient distortion. IEEE Antennas and Wireless Propagation Letters. 2011;10: 302–305.

[14] Jongh RK, Hajian M, Ligthart LP. Antenna Time–Domain Measurement Techniques. IEEE Antennas and Propagation Magazine. 1997 October;39 (5):7–12.

[15] Shlivinski A, Heyman E, Kastner R. Antenna characterization in the Time Domain. IEEE Transactions on Antennas and Propagation. 1997;45(7): 1140–1149.

[16] Sorgel W, Knorzer S, Wiesbeck W. Measurement and Evaluation of ultra wideband antennas for communications. In: International ITG Conference on Antennas – INICA2003. Germany; 2003. p. 377–380.

[17] Sorgel W, Weisbeck W. Influence of the antennas on the ultra–wideband transmission. EURASIP Journal on Applied Signal Processing. 2005;3: 296–305.

[18] Zwierzchowski S, Jazayeri P. Derivation and determination of the antenna transfer function for use in ultra–wideband communications analysis. Wireless Proceedings. 2003 July;.

[19] Mohammadian AH, Rajkotia A, Soliman SS. Characterization of UWB transmit–receive antenna system. In: IEEE Conf. Ultra Wideband Systems and Technology; 2003. p. 157–161.

[20] Duroc Y, Ghiotto A, Vuong TP, Tedjini S. UWB Antennas: Systems With Transfer Function and Impulse Response. IEEE Transaction on Antennas and Propagation. 2007 May;55 (5):1449–1451.

[21] Telzhensky N, Leviatan Y. Novel Method of UWB Antenna Optimization for Specified Input Signal Forms by Means of Genetic Algorithm. IEEE Transaction on Antennas and Propagation. 2006 August;54(8): 2216–2225.